Funnel-based biomimetic volume optics

E. DelRe,[1,2,*] **A. Pierangelo,**[3] **J. Parravicini,**[1,2] **S. Gentilini,**[1,4] **and A. J. Agranat**[5]

[1]*Department of Physics, University of Rome "La Sapienza", 00185 Rome, Italy*
[2]*Department of Electrical Engineering, University of L'Aquila, 67100 L'Aquila, Italy*
[3]*LPICM, Ecole Polytechnique, CNRS, 91128 Palaiseau, France*
[4]*ISC-CNR, University of Rome "La Sapienza", 00185 Rome, Italy*
[5]*Applied Physics Department, Hebrew University of Jerusalem, Jeusalem 91904, Israel*

[*]*eugenio.delre@uniroma1.it*

Abstract: We demonstrate the use of three-dimensional funnel index of refraction patterns analogous to those of retinal Müller cells as support for tunable and multi-functional volume optical component miniaturization and integration. Our experiments in paraelectric photorefractive crystals show how a single funnel can act both as a waveguide and a tunable focusing/defocusing micro-lens. Pairing multiple funnel patterns, we are also able to demonstrate ultra-compact tunable beam-splitting, with distinct guided output modes in under 1mm of propagation.

© 2012 Optical Society of America

OCIS codes: (190.6135) Spatial solitons; (200.4650) Optical interconnects; (230.3120) Integrated optics devices; (250.6715) Switching.

References and links

1. K. Franze, J. Grosche, S. N. Skatchkov, S. Schinkinger, C. Foja, D. Schild,O. Uckermann, K. Travis, A. Reichenbach, and J. Guck, "Muller cells are living optical fibers in the vertebrate retina," Proc. Nat. Acad. Sci. USA **104**, 8287–8292 (2007).
2. A. M. Labin and E. N. Ribak, "Retinal glial cells Enhance human vision acuity," Phys. Rev. Lett. **104**, 158102 (2010).
3. E. DelRe, A. Pierangelo, E. Palange, A. Ciattoni, and A. J. Agranat, "Beam shaping and effective guiding in the bulk of photorefractive crystals through linear beam dynamics," Appl. Phys. Lett. **91**, 081105 (2007).
4. A. Pierangelo, E. DelRe, A. Ciattoni, E. Palange, A. J. Agranat, and B. Crosignani, "Linear writing of waveguides in bulk photorefractive crystals through a two-step polarization sequence," J. Opt. A. Pure Appl. Opt. **10**, 064005 (2008).
5. A. Pierangelo, A. Ciattoni, E. Palange, A. J. Agranat, and E. DelRe, "Electro-activation and electro-morphing of photorefractive funnel waveguides," Opt. Express **17**, 22659–22665 (2009).
6. N. J. Cerf, C. Adami, and P. G. Kwait, "Optical simulation of quantum logic," Phys. Rev. A **57**, R1477–R1480 (1998).
7. A. Politi, M. J. Cryan, J. G. Rarity, S. Yu, and J. L. O'Brien, "Silica-on-silicon waveguide quantum circuits," Science **320**, 646–649 (2008).
8. A. Crespi, R. Ramponi, R. Osellame, L. Sansoni, I. Bongioanni, F. Sciarrino, G. Vallone, and P. Mataloni, "Integrated photonic quantum gates for polarization qubits," Nat. Commun. **2**, 566 (2011).
9. Y. Frauel and B. Javidi, "Neural network for three-dimensional object recognition based on digital holography," Opt. Lett. **26**, 1478–1480 (2001).
10. R. Heintzmann and M. G. L. Gustafsson, "Subdiffraction resolution in continuous samples," Nat. Photonics **3**, 362–364 (2009).
11. S. Popoff, G. Lerosey, M. Fink, A. C. Boccara, and S. Gigan, "Image transmission through an opaque material," Nat. Commun. **1**, 81 (2010).
12. D. Marcuse, *Theory of Dielectric Optical Waveguides* (Academic Press, New York, 1974).
13. K. Miura, J. Qiu, H. Inouye, and T. Hirao, "Photowritten optical waveguides in various glasses with ultrashort pulse laser," Appl. Phys. Lett. **71**, 3329–3331 (1997).
14. W. Torruellas and S. Trillo (eds.), *Spatial Solitons*, (Springer, New York, 2001).

#162855 - $15.00 USD Received 10 Feb 2012; revised 30 May 2012; accepted 1 Jun 2012; published 9 Jul 2012
(C) 2012 OSA

15. T. M. Monro, C. M. De Sterke, and L. Poladian, "Self-writing a waveguide in glass using photosensitivity," Opt. Commun. **119**, 523–526 (1995).
16. S. Kewitsch and A. Yariv, "Self-focusing and self-trapping of optical beams upon photopolymerization," Opt. Lett. **21**, 24–26 (1996).
17. K. Dorkenoo, O. Cregut, L. Mager, F. Gillot, C. Carre, and A. Fort, "Quasi-solitonic behavior of self-written waveguides created by photopolymerization," Opt. Lett. **27**, 1782–1784 (2002).
18. M. Morin, G. Duree, G. Salamo, and M. Segev, "Waveguides formed by quasi-steady-state photorefractive spatial solitons," Opt. Lett. **20**, 2066–2068 (1995).
19. E. DelRe, M. Tamburrini, and A. J. Agranat, "Soliton electro-optic effects in paraelectrics," Opt. Lett. **25**, 963–965 (2000).
20. E. DelRe, B. Crosignani, E. Palange, and A. J. Agranat, "Electro-optic beam manipulation through photorefractive needles," Opt. Lett. **27**, 2188–2190 (2002).
21. M. Asaro, M. Sheldon, Z. G. Chen, O. Ostroverkhova, and W. E. Moerner, "Soliton-induced waveguides in an organic photorefractive glass," Opt. Lett. **30**, 519–521 (2005).
22. M. Chauvet, A. Q. Gou, G. Y. Fu, and G. Salamo, "Electrically switched photoinduced waveguide in unpoled strontium barium niobate," J. Appl. Phys. **99**, 113107–113112 (2006).
23. M. H. Chou, M. A. Arbore, and M. M. Fejer, "Adiabatically tapered periodic segmentation of channel waveguides for mode-size transformation and fundamental mode excitation," Opt. Lett. **21**, 794–796 (1996).
24. C. Dari-Salisburgo, E. DelRe, and E. Palange, "Molding and stretched evolution of optical solitons in cumulative nonlinearities," Phys. Rev. Lett. **91**, 263903–263906 (2003).
25. E. DelRe and E. Palange, "Optical nonlinearity and existence conditions for quasi-steady-state photorefractive solitons," J. Opt. Soc. Am. B **23**, 2323–2327 (2006).
26. A. Yariv, *Q*uantum Electronics, 3rd ed. (Wiley, New York, 1988).
27. A. Agranat, R. Hofmeister, and A. Yariv, "Characterization of a new photorefractive material: Kl-yLyT1-xNx," Opt. Lett. **17**, 713–715 (1992).
28. W. Krolikowski, M. Saffman, B. Luther-Davies, and C. Denz, "Anomalous interaction of spatial solitons in photorefractive media," Phys. Rev. Lett. **80**, 3240–3243 (1998).
29. E. DelRe, A. Ciattoni, and A. J. Agranat, "Anisotropic charge displacement supporting isolated photorefractive optical needles," Opt. Lett. **26**, 908–910 (2001).
30. E. DelRe, G. De Masi, A. Ciattoni, and E. Palange, "Pairing space-charge field conditions with self-guiding for the attainment of circular symmetry in photorefractive solitons," Appl. Phys. Lett. **85**, 5499–5501 (2004).

1. Introduction

In many situations light must be collected, guided, and then delivered efficiently to photoreceptors through a volume. This is what occurs in the vertebrate eye, where light must be funnelled through a mangled mass of scattering tissue before reaching the retinal detectors. Recent studies suggest that light transmission is effected by Müller cells [1]. In distinction to conventional waveguides, that are essentially tubular, these cells have a *double-funnel shape*. This shape allows them to efficiently focus, collect, transfer, and outcouple light without the strong mode selectivity of waveguides. Moreover, their shape profoundly alters inter-channel cross-talk compared to waveguide arrays [2]. Here we explore the use of biologically inspired funnel index of refraction patterns that mimic retinal Müller cells as versatile volume blueprints for multiple optical functions, including optical guiding, lensing, mode-conversion and compact beam splitting. The result is a generic support for the volume integration of optical components for highly miniaturized optical networks, where diffraction transforms light transfer into a major challenge. Our experiments are based on a two-stage index of refraction pattern writing/reading process developed in photorefractive crystals [3–5]. Funnels can prove the scheme of choice for experiments where solid-state miniaturization is a future imperative, such as for optical quantum computing [6–8], pattern recognition [9], pattern formation for microscopy [10], and imaging techniques [11].

2. Mechanism and model: a tunable distributed lensing

The common route to volume integration is to start from the waveguide paradigm, a duct that guides micrometer-sized beams with no distortion [12]. How exactly to make a waveguide em-

#162855 - $15.00 USD Received 10 Feb 2012; revised 30 May 2012; accepted 1 Jun 2012; published 9 Jul 2012
(C) 2012 OSA

bedded deep in the volume of a material is of course an issue in itself. One solution is to proceed through sequential writing of the pattern [13]. Another is the self-writing of waveguides supported by spatial soliton propagation [14], a well established technique in many photosensitive materials [15–17] and in photorefractive crystals [18]. Photorefractive soliton waveguides can also be activated on command through the electro-optic effect [19–22].

All these schemes are based on a shape-preserving tube-like channel. This paradigm is ill-fit to form a *generic* support for optical components. For example, switching using waveguides requires the use of directional-coupling, an interferometric mechanism that is both wavelength sensitive and requires comparatively long propagation lengths. More so, whereas a lens will readily change the shape and size of a beam, to achieve this in a *waveguide* requires more delicate mode conversion or the use of tapered structures [23].

Müller cells suggest a wholly different mechanism to achieved a more general and versatile optical functionality: the use of a funnel-shaped index of refraction pattern instead of a waveguide. Compared to tube-like patterns typical of soliton-based waveguides, funnels are fully three-dimensional structures (illustrated in Fig. 1(a)). In the vertebrate eye, the elongated double-funnel pattern achieves at once focusing, guiding, and defocusing: the key ingredient is the changing shape along the propagation direction (say the z axis) that can, depending on circumstances, act as a lens (the cellular "end-feet"), or as a fiber (the cellular "body"), thus forming a basic blueprint to multifunctional optics [1, 2].

Here we make use of funnel index or refraction patterns in photorefractive crystals [3–5]. Consider a biased photorefractive crystal into which we shine a highly diffracting Gaussian visible laser beam (propagating along the z axis). During a first phase, that we may term the "exposure phase", light promotes electrons from the photorefractive impurities that drift in the external bias field E_0 oriented along the x axis and retrap in deep in-band donor sites. This gives rise to a space-charge field E_{sc} that, in standard conditions, changes beam diffraction through the electro-optic effect. We inhibit electro-optic response by orienting the polarization of the optical field in the y direction, orthogonal to E_0. In this manner, during this exposure phase, the beam diffracts as it would in a homogeneous linear medium, producing the funnel-like E_{sc}. This is because the direction of E_0 fixes the prevalent direction of E_{sc} parallel to the x-axis, and the electro-optic response for light polarized in the orthogonal plane is generally negligible. Once the exposure of a desired duration t_e has terminated, the blue-print is fixed in the crystal. The exposed region in the crystal is now used to affect the propagation of light polarized along the x direction, i.e., parallel to E_0. In this case, the electro-optic response is maximized, since the low-frequency electric field in the crystal and the polarization of the propagating light are parallel. In this "readout phase", E_{sc} is kept fixed. This is achieved using a low intensity visible beam, so that promotion of conduction electrons from the photorefractive impurities is negligible. Equally effective is the use of longer wavelength beams which simply cannot ionize the deep impurities.

In our conditions, the photorefractive model provides an index of refraction response [3] that is the direct analog of the wider class of photosensitive materials, such as photopolymers [16], for which the crystal index of refraction n_b is changed to $n = n_b + \Delta n$, where

$$\Delta n(\mathbf{r}, t_e) = \Delta n_0 e^{-\frac{1}{U_0} I(\mathbf{r}) t_e}. \tag{1}$$

Here $I(\mathbf{r})$ is the spatially resolved intensity distribution of the diffracting Gaussian beam in the exposure phase, and U_0 is the critical exposure. In the case of a quadratic electro-optic response (only insignificant details change for a linear electro-optic response), $\Delta n_0 = -(1/2) n_b^3 g_{11} \varepsilon_0^2 (\varepsilon_r - 1)^2 E_0^2$ and $U_0 = I_b \tau_d / 2$, where g_{11} is the principal quadratic electro-optic coefficient, ε_r is the low frequency relative dielectric constant, I_b is the so-called dark illumination associated to the residual thermal excitation of mobile electrons, and τ_d is the dielectric

#162855 - $15.00 USD Received 10 Feb 2012; revised 30 May 2012; accepted 1 Jun 2012; published 9 Jul 2012
(C) 2012 OSA

relaxation time [24, 25]. Specifically, $\tau_d = \varepsilon_0 \varepsilon_r \gamma N_a / [q\mu s(N_d - N_a) I_b]$, where N_a and N_d are the density of acceptor and donor impurities, respectively, q is the electron charge, γ is the electron recombination rate, μ is the electron mobility in the conduction band, and s is the ionization cross-section for the donor sites.

The basic mechanism underlying components arising from the funnel blueprint can best be grasped identifying the pattern as a versatile propagation-dependent distributed lensing effect. Consider a Gaussian beam in the exposure phase centered in (x_0, y_0), $I = (I_p/G(z)) \exp(-2r^2/w_0^2 G(z))$, where I_p is the beam peak intensity, $G(z) = 1 + (z - z_c)^2/z_0^2$, z_c is the position of the minimum beam waist along the propagation direction z, $z_0 = n_b \pi w_0^2/\lambda$ is the diffraction length, w_0 is the beam waist, λ is the optical wavelength, and $r^2 = (x - x_0)^2 + (y - y_0)^2$. In the readout phase, in conditions in which the beam is focused and guided, light propagates in proximity of the axis of the funnel footprint (the E_{sc} previously imprinted by the diffracting writing beam) so that $r^2/w_0^2 G(z) \ll 1$ and, from Eq. (1), we have

$$\Delta n \simeq H(z) r^2, \tag{2}$$

where only the modulated part of Δn is retained (the constant terms do not affect beam dynamics). Here

$$H(z) = \Delta n_0 \exp(-a/G(z)) 2a/(w_0^2 G(z)^2) \tag{3}$$

and $a = t_e I_p/U_0$. $H(z)$ determines the nature of the emerging component from the funnel E_{sc} support. Equation (2) means that the funnel acts like a distributed lensing with a z-dependent focal length, centered at (x_0, y_0), with $f(z) \propto 1/H(z)$. The pattern has two main features: i) given Eq. (2), it will transform Gaussian beams into Gaussian beams, so that diffraction-limited solutions will be maintained throughout propagation [26]; and ii) through $H(z)$ the actual lens-like medium can be designed and tailored to give rise to a wanted component by fixing the set of controllable parameters $(a, z_c, \Delta n_0, w_0)$. Notably, a can be actively controlled during the writing stage simply by changing t_e. Examples of patterns are reported in Fig. 1(b). Different values of a provide different distributed lensing effects. Unsaturated cases, that is, for $a < 1$, give rise to parabolic-like lensing that can be used to achieve tunable lenses and mode converters. For $a = 1 \div 2.5$, a waveguide emerges for $|z/z_c| \leq 1$, the very same mechanism known in Müller cells [1]. For $a > 2.5$ a more complex lensing occurs which is instrumental for mode conversion, mode coupling, and beam splitting.

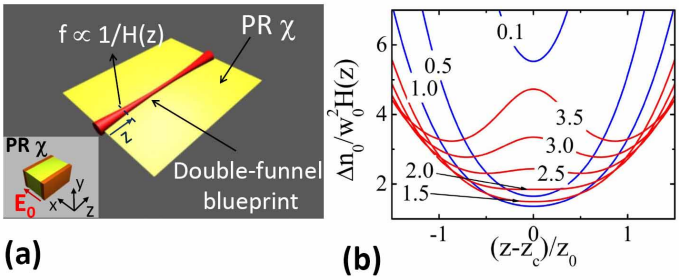

Fig. 1. Funnel patterns and distributed lensing. (a) Schematic of funnel support. Inset shows the experimental geometry, with the direction of the applied electric field $\mathbf{E}_0$ with respect to the photorefractive crystal (PRχ) (b) Different distributed lensing patterns for various values of a (the focal length of the lensing effect at a given position z along the double-funnel is $f \propto 1/H(z)$). Blue curves are for the unsaturated cases ($a < 1$) and red for the saturated cases ($a > 1$).

#162855 - $15.00 USD Received 10 Feb 2012; revised 30 May 2012; accepted 1 Jun 2012; published 9 Jul 2012
(C) 2012 OSA

3. Electro-morphing.

Fast changes in the pattern and its functionality are achieved applying a bias field $E_0' \neq E_0$ (during the readout phase). In this case, the space-charge field nonlinearly combines with the applied bias field to give rise to an approximate parabolic profile (as in Eq. (2)) $\Delta n(E_0') \simeq H'(z)r^2$ (dropping all r-independent terms) with

$$H'(z) = H(z)\left[1 + \left(E_0'/E_0 - 1\right)\exp\left(a/2G(z)\right)\right]. \tag{4}$$

This is the equivalent, in the present funnel-pattern case, of the electro-activated pattern at the basis of electro-holography and soliton electro-activation. We illustrate in Fig. 2 two relevant examples of the various patterns that can be electro-morphed from a single parent double-funnel E_{sc} support. Increasing $|E_0'|$ will, in general, reduce the z-dependence, leading to waveguiding, whereas changing the polarization of the bias ($E_0'/E_0 < 0$) gives rise to distributed defocusing structures. We note that in the defocusing case the simplified physical picture based on a distributed lens-like medium loses its validity as the beam expands and explores the edges of the funnel pattern. In this case, the full model of Eq. (1) is required.

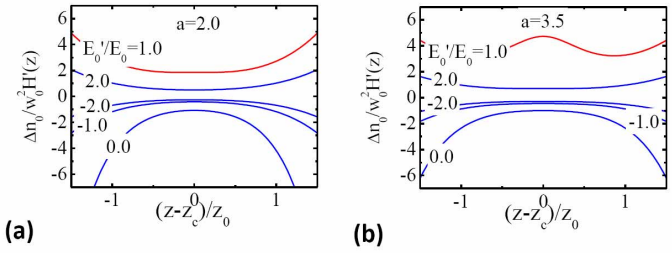

Fig. 2. Electro-morphing. (a) Different distributed lensing patterns for various values of E_0'/E_0 and $a = 2.0$ (the focal length of the lensing effect at a given position z along the double-funnel is $f \propto 1/H'(z)$); (b) for $a = 3.5$. Note the transition from a positive to a negative distributed lensing effect.

4. Experimental

Experiments are carried out in a $2.4^{(x)}$x$3.0^{(y)}$x$1.0^{(z)}$ mm sample of Cu-doped KLTN (potassium-lithium-tantalate-niobate) [27], kept at $T = 19°$C, above its ferroelectric Curie point at $T_C = 14°$C. During the exposure phase, a 800 nW TEM_{00} beam of $\lambda = 543$ nm polarized along the y direction is launched from a He-Ne laser in the z direction, focused down to a round spot size of $\Delta x \simeq \Delta y \simeq 7.5\ \mu$m (i.e., of $w_0 \simeq 6.3\mu$m) at the minimum waist plane at z_c. The input and output beam intensity distribution is monitored through a CCD camera and an appropriate imaging system. Bias fields range from $E_0 = -4.6$kV/cm to $+4.6$ kV/cm, so that the amplitude of the index modulation is here $\Delta n \sim (1/2)n_b^3\varepsilon_0^2\varepsilon_r^2 g_{12}E_0^2 \sim 3\times10^{-5}$, where $n_b = 2.35$, $\varepsilon_r = \varepsilon_r(T) = 1.9\times10^4$, and $g_{12} = -0.02\text{m}^4\text{C}^{-2}$ is the component of the quadratic electro-optic tensor that induces changes for the y-polarization and the x-directed field E_0: as required, this value is insufficient to appreciable alter the diffraction. In the readout phase, the reading beam is attained from the same beam used in the writing phase but with an intensity reduced to 10 nW, so that the resulting exposure (and nonlinearity) becomes negligible. The beam is consistently focused onto the input facet of the sample, and the optical polarization is rotated in the x direction so that the relevant electro-optic coefficient is $g_{11} = 0.16\text{m}^4\text{C}^{-2}$. In these conditions, the $\Delta n_0 \sim 4\cdot10^{-4}$ is now capable of profoundly altering beam dynamics, that occur on the scale $z_0 = n_b\pi w_0^2/\lambda \simeq 530\mu$m. In our results we analyze the output beam

#162855 - $15.00 USD Received 10 Feb 2012; revised 30 May 2012; accepted 1 Jun 2012; published 9 Jul 2012
(C) 2012 OSA

sizes, the full-width-at-half-maximum, for different exposure times t_e. Values of t_e are then converted to values of a by comparison to predictions of the lens-like model. Specifically, by setting the value of $a = 2.5$ when the condition of approximate waveguiding in observed, we obtain $a/t_e = 2I_p/\tau_d I_b \simeq 0.17\text{s}^{-1}$.

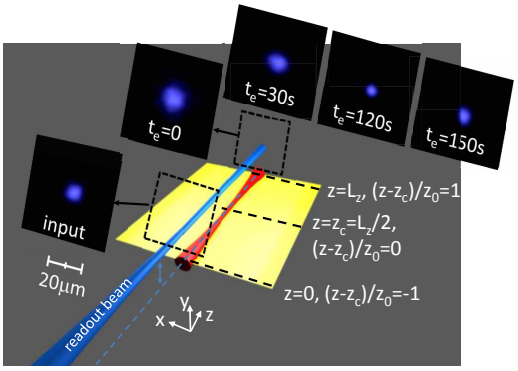

Fig. 3. Lensing and waveguiding using funnels. Results of readout with $E_0'/E_0 = 1$ for a beam propagating in along the z-axis for different exposure times, for $z_c = L_z/2$. First image starting from left is the input intensity distribution, whereas the others that follow are of the output intensity distribution.

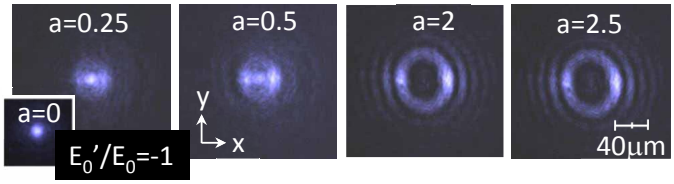

Fig. 4. Electro-morphing into a defocusing pattern for $E_0'/E_0 = -1$ at various values of a. The images report the output intensity distribution during readout. The $a = 0$ condition is identical to that reported in the previous Fig. (3).

From lensing to waveguiding through saturation control. A basic result is when $a = 2.5$. In this case, as shown in the prediction of Fig. 1(b), a constant distributed lensing forms, leading to a waveguide. For $z_c = 0$ we will call the configuration a single-funnel waveguide; for $z_c = L_z/2$, we will refer to it as a double-funnel waveguide. In Fig. 3 we report results on the generation of a double-funnel lensing and double funnel waveguide. The writing phase is characterized by a constant voltage $V = 1.1\text{kV}$ (so that $E_0 = 4.6\text{kV/cm}$) for the whole duration t_e. Compared to the diffracting beam ($a = 0$), the $a = 0.5$ clearly manifests a lensing effect, that is actually able to make the beam smaller during the propagation at $a = 2.0$. As saturation sets in (red curves in Fig. 1), the focusing gives way to a waveguiding (see the $a = 2.5$ case in Fig. 3), as expected from the model. Detecting the far-field of the transmitted beams we established that all beams were approximately still diffraction-limited Gaussian solutions. Specifically, in the $a = 2.5$ of waveguiding, we measured the diffraction of the beam after exiting the crystal and found it to

#162855 - $15.00 USD Received 10 Feb 2012; revised 30 May 2012; accepted 1 Jun 2012; published 9 Jul 2012
(C) 2012 OSA

be compatible with Gaussian beam diffraction with a minimum beam waist at the output facet of the sample.

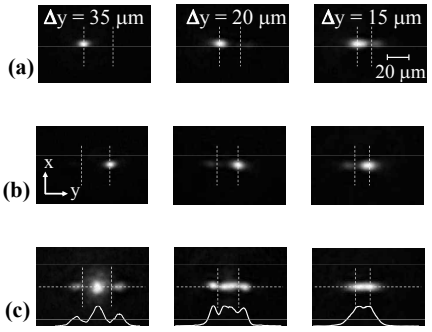

Fig. 5. Ultra-compact beam splitting through two parallel funnel patterns for $a = 3$, $z_c = 0$ for different levels of compacting Δy. (a) Output intensity distribution of the read-out beam guided by the first funnel; (b) output of beam guided by the second funnel; (c) output of the two-funnel pattern for the read-out beam launched in between the two funnels with normalized beam intensity profile in the y direction. The absence of efficient beam-splitting in all cases of compacting is evident, whereas a form of super-mode emerges in the $\Delta y = 15\mu$m case.

Electromorphing into anti-lensing and antiguiding patterns. The most evident result of the electro-morphing described in Fig. 2 is the ability to turn a funnel pattern from a lensing or guiding pattern to an anti-lensing and antiguiding pattern. Accordingly, in Fig. 4 we report experiments in which the double-funnel pattern is written as in the previous lensing experiments but the bias field during read-out is such that $E_0'/E_0 = -1$ (i.e., the applied voltage V is reversed). In agreement with the model of electro-morphing, for unsaturated values of a such as $a = 0.25, 0.5$, the effect is a defocusing of the Gaussian mode, from the original $\Delta x \simeq \Delta y \simeq 15\mu$m (for $a = 0$) to 32 and 40 μm respectively, this in L_z =1 mm of propagation. This corresponds to a passage from a numerical aperture of NA($a = 0$)$\simeq 0.01$ to NA($a = 0.5$)$\simeq 0.04$ ($n_b = 2.35$). Evidently, as reported in Fig. 4, for saturated values of $a = 2, 2.5$, this defocusing gives way to an antiguiding effect, the reverse of the guiding effect reported in Fig. 3. As mentioned previously, the highly delocalized beam condition requires the full model of Eq. (1).

Ultra-compact beam-splitting and the role of the three-dimensional funnel shape. In Fig. 5 and Fig. 6 we demonstrate the use of coupled funnel patterns to achieve ultra-compact beam splitting. In Fig. 5 we realize two funnel patterns with $z_c = 0$ and $a = 3$. We displace the two funnel patterns in the y direction in order to avoid the residual anisotropy in the photorefractive response, anisotropy that so greatly affects photorefractive soliton formation and electro-optic read-out [28–30]. For different values of compacting $\Delta y = 35, 20, 15\mu$m (first, second and third columns in Fig. 5) we note evidence of energy transfer between the funnel patterns that, however, does not lead to an efficient beam splitting, as reported in Fig. 5(c). However, using the full strength of the funnel pattern in Fig. 6, where $z_c = L_z/2$ and again $a = 3$, in the $\Delta y = 15\mu$m case full 50/50 beam splitting is observed, with no residual mode overlap. This occurs in the remarkably short propagation of $L_z = 1$ mm and the output beams are in fact approximately

#162855 - $15.00 USD Received 10 Feb 2012; revised 30 May 2012; accepted 1 Jun 2012; published 9 Jul 2012
(C) 2012 OSA

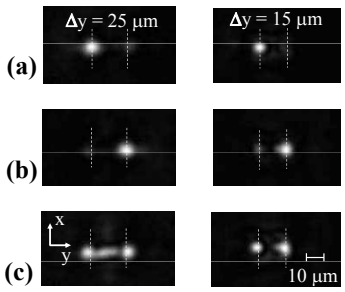

Fig. 6. Ultra-compact beam splitting through two parallel funnel patterns for $a = 3$, $z_c = L_z/2$. The role of the three dimensional nature of the patterns is evident comparing the effect at two different inter-funnel distances $\Delta 25\mu$m (left column) and $\Delta 15\mu$m (right column). (a) Output intensity distribution of the read-out beam guided by the first funnel; (b) output of beam guided by the second funnel; (c) output of the two-funnel pattern for the read-out beam launched in between the two funnels.

guided, as detected through the analysis of diffraction in the far-field. The comparison of the $z_c = 0$ and $z_c = L_z/2$ for various levels of compacting Δy forms the signature of the role of the three-dimensional shape of the funnels, as also predicted in Müller cell mutual coupling.

5. Conclusion

We demonstrate the realization and implementation of a tunable distributed lensing effect in photorefractive crystals. The lensing is based on a funnel three-dimensional pattern analogous to that found in in glial cells in the retina, and is shown to act as a waveguide (constant distributed lensing), a positive or negative lens, a mode converter and a coupler, with remarkably short millimetric splitting and coupling lengths. Results can form the basis for more elaborate fully three-dimensional optical circuitry for light control in highly miniaturized environments that are dominated by strong diffraction.

Acknowledgments

This work was supported by funding from the Italian Ministry of Research (MIUR) through the "Futuro in Ricerca" FIRB grant PHOCOS-RBFR08E7VA. Partial funding was received through the SMARTCONFOCAL project of the Regione Lazio and through the PRIN project no. 2009P3K72Z. A.J.A. acknowledges the support of the Peter Brojde Center for Innovative Engineering.

#162855 - $15.00 USD Received 10 Feb 2012; revised 30 May 2012; accepted 1 Jun 2012; published 9 Jul 2012
(C) 2012 OSA